Acta Crystallographica Section D
Biological Crystallography
ISSN 0907-4449

Systematic study on crystal-contact engineering of diphthine synthase: influence of mutations at crystal-packing regions on X-ray diffraction quality

Hisashi Mizutani,[a] K. Saraboji,[b] S. M. Malathy Sony,[b] M. N. Ponnuswamy,[b] T. Kumarevel,[a] B. S. Krishna Swamy,[c] D. K. Simanshu,[c] M. R. N. Murthy[c] and Naoki Kunishima[a]*

[a]RIKEN SPring-8 Center, Harima Institute, 1-1-1 Kouto, Sayo-cho, Sayo-gun, Hyogo 679-5148, Japan, [b]Department of Crystallography and Biophysics, University of Madras, Guindy Campus, Chennai 600025, India, and [c]Molecular Biophysics Unit, Indian Institute of Science, Bangalore 560012, India

Correspondence e-mail: kunisima@spring8.or.jp

Received 12 April 2008
Accepted 22 July 2008

PDB References: diphthine synthase, 1wng, r1wngsf; K26R, 2dsg, r2dsgsf; K26Y, 2dsh, r2dshsf; K49R, 2z6r, r2z6rsf; E54H, 2dxv, r2dxvsf; E54K, 2dxw, r2dxwsf; E54R, 2e7r, r2e7rsf; L65A, 2dv5, r2dv5sf; L65Q, 2dv4, r2dv4sf; N69K, 2ehc, r2ehcsf; D79E, 2e07, r2e07sf; E140K, 2e08, r2e08sf; E140N, 2egb, r2egbsf; E140R, 2e16, r2e16sf; N142E, 2dxx, r2dxxsf; T146R, 2ehl, r2ehlsf; E171K, 2egl, r2eglsf; E171R, 2dsi, r2dsisf; R173A, 2e17, r2e17sf; R173N, 2e15, r2e15sf; K187R, 2dv7, r2dv7sf; L261M, 2egs, r2egssf.

It is well known that protein crystallizability can be influenced by site-directed mutagenesis of residues on the molecular surface of proteins, indicating that the intermolecular interactions in crystal-packing regions may play a crucial role in the structural regularity at atomic resolution of protein crystals. Here, a systematic examination was made of the improvement in the diffraction resolution of protein crystals on introducing a single mutation of a crystal-packing residue in order to provide more favourable packing interactions, using diphthine synthase from *Pyrococcus horikoshii* OT3 as a model system. All of a total of 21 designed mutants at 13 different crystal-packing residues yielded almost isomorphous crystals from the same crystallization conditions as those used for the wild-type crystals, which diffracted X-rays to 2.1 Å resolution. Of the 21 mutants, eight provided crystals with an improved resolution of 1.8 Å or better. Thus, it has been clarified that crystal quality can be improved by introducing a suitable single mutation of a crystal-packing residue. In the improved crystals, more intimate crystal-packing interactions than those in the wild-type crystal are observed. Notably, the mutants K49R and T146R yielded crystals with outstandingly improved resolutions of 1.5 and 1.6 Å, respectively, in which a large-scale rearrangement of packing interactions was unexpectedly observed despite the retention of the same isomorphous crystal form. In contrast, the mutants that provided results that were in good agreement with the designed putative structures tended to achieve only moderate improvements in resolution of up to 1.75 Å. These results suggest a difficulty in the rational prediction of highly effective mutations in crystal engineering.

1. Introduction

In recent years, a huge number of protein crystal structures have been determined using the high-throughput facilities developed by the efforts of structural genomics initiatives. For instance, a encyclopaedic structural analysis program on the extreme thermophile *Thermus thermophilus* HB8 was performed as part of the Japanese structural genomics project 'National Project on Protein Structural and Functional Analyses (Protein 3000 Project)' from April 2002 to March 2007 (Yokoyama *et al.*, 2002). To date, structure determination has been completed for over 20% of the 2200 proteins from the *T. thermophilus* genome. Therefore, as far as the three-dimensional structure of proteins is concerned, *T. thermophilus* can now be regarded as the most extensively analyzed organism. However, the remaining ~80% of the proteins are difficult to analyze using current protein-crystallography

© 2008 International Union of Crystallography
Printed in Singapore – all rights reserved

technology. These difficult target proteins, which include membrane proteins and supramolecular complexes, usually have problems with stability and/or molecular-surface properties such as flexible loops and hydrophobic patches, thereby providing crystals with poor diffraction quality in many cases. Furthermore, even an extremely stable and 'firm' protein cannot be crystallized if it does not have a molecular surface that is favourable for crystal packing. Therefore, in order to promote the structural analysis of difficult targets, a methodological development for the improvement of crystal quality is an inevitable task in protein crystallography.

Site-directed mutagenesis has been used to improve the crystallizability of proteins in cases where crystallization was unsuccessful using conventional screening methods. The crystal structure determination of human H-chain ferritin (Lawson *et al.*, 1991) was one of the first successful examples of such a site-directed mutagenesis experiment, in which the mutation was designed based on the crystal structures of rat and horse L-chain ferritins, which were known to bind Cd^{2+} ions at their intermolecular crystal-packing regions. In the human H-chain ferritin, the introduction of a K86Q mutation at the residue corresponding to that responsible for Cd^{2+} binding in the rat and horse proteins successfully induced a similar metal bridge in the crystals of human protein and allowed structure determination. Around the same time, the influence of mutations of molecular-surface residues on protein crystallization was investigated for the first time; single-site surface mutants of human thymidylate synthase provided various crystals with different crystal-packing patterns (McElroy *et al.*, 1992). Later, a similar investigation of surface mutation was performed on DNA gyrase B subunit, in which a mutant crystal showed improved X-ray diffraction resolution compared with the wild-type crystal, although further structural comparison was not available (D'Arcy *et al.*, 1999). Very recently, several new crystallization methods using molecular-surface mutations have been reported: the artificial introduction of intermolecular disulfide bonds by Cys mutations (Banatao *et al.*, 2006), intermolecular leucine-zipper formation by Leu mutations (Yamada *et al.*, 2007) and the replacement of flexible surface residues such as Lys, Glu and Gln by other residues with small side chains, referred to as the 'surface-entropy reduction' (SER) method (Cooper *et al.*, 2007). The SER method thermodynamically promotes protein crystallization by reducing the conformational entropy of surface residues, considering that molecular-surface residues with disordered side chains have high conformational entropy in the solution state and thereby produce an unfavourable negative entropy change if they become ordered at crystal-packing regions in the crystalline state.

Notably, most of the mutation sites in these successful experiments were found at crystal-packing contact regions, suggesting that the atomic level regularity of protein crystals is in general dominated by crystal-packing interactions. Thus, appropriate modification of crystal-packing contacts by site-directed mutagenesis may in principle be effective in improving the quality of the protein crystals. However, the mutations in the reported mutational studies were not introduced at known crystal-contact residues. Therefore, additional crystallization screening for the mutant protein is required in these cases, which is semantically equivalent to the independent structural determination of a novel protein. This re-screening of crystallization conditions may not be necessary if a mutational modification of unfavourable protein–protein interactions at previously known crystal contacts can help in structural determination. This idea has never been examined to date, probably owing to the absence of an applicable model system that would allow quantitative investigation of the relationship between mutation and crystal quality. Here, we have established such a model system using diphthine synthase from *Pyrococcus horikoshii* OT3 (*Ph*DS) and succeeded in evaluating the influence of mutations at crystal-packing regions on X-ray diffraction quality. The *Ph*DS system has several favourable characteristics for the present investigation. Firstly, *Ph*DS is of medium molecular size for a protein (a homodimer of two protomers with 265 amino-acid residues each), which is an important factor when the results are applied to other proteins. Since the wild-type crystal structure (PDB code 1wng; Kishishita *et al.*, 2008) was determined at 2.1 Å resolution, the *Ph*DS system would be appropriate to evaluate how the resolution is affected by the amino-acid substitution. Furthermore, most of the mutants could be expressed easily and provided sufficient quantities of protein sample for structural analysis. The most important property of this system is the robustness of the crystal form upon mutation; most of the mutants yielded nearly isomorphous crystals from the same crystallization condition as used for the wild-type protein. In this report, a systematic study of crystal-contact engineering is represented based on the crystal structures of 21 mutant proteins from the *Ph*DS system.

2. Materials and methods

2.1. Mutagenesis and production of *Ph*DS

Site-directed mutagenesis was performed using the QuikChange mutagenesis kit (Stratagene). Native *Ph*DS was used as a template and the DNA sequence of the mutant plasmid was confirmed after mutagenesis. Protein expression and purification were performed as follows by the Structurome Research Group of the RIKEN SPring-8 Center. *Escherichia coli* BL21 CodonPlus (DE3)-RIL cells were transformed with the mutant plasmid and grown without IPTG induction at 310 K in LB medium containing 50 µg ml^{-1} ampicillin for 20 h. The cells were harvested by centrifugation at 20 000*g* for 5 min, suspended in 20 m*M* Tris–HCl pH 8.0 (buffer *A*) containing 0.5 *M* NaCl, 5 m*M* 2-mercaptoethanol and 1 m*M* phenylmethanesulfonylfluoride and subsequently disrupted by sonication. The cell lysate was heated to 363 K for 13 min. After the heat treatment, denaturated proteins were removed by centrifugation (21 600*g*, 30 min) and the supernatant solution was used as the crude extract for purification. The crude extract was desalted using a HiPrep 26/10 desalting column (Amersham Biosciences) and applied onto a Super Q Toyopearl 650M column (Tosoh) equilibrated with buffer *A*.

Table 1
Summary of *Ph*DS mutant crystal structures determined in this study.

Protein	Related symmetry	Contact modifications†		Resolution (Å)	R_{work}/R_{free} (%)	R.m.s.d. on C^{α} superposition (Å)	Rigid-body rotation in asymmetric unit (°)	PDB code
		Expected	Results					
Wild type				2.1	19.8/22.8			1wng
K26R	4_1	1	1	2.0	18.8/21.1	0.107	0.47	2dsg
K26Y	4_1	1	1, 2, −5	2.0	19.4/21.8	0.152	1.07	2dsh
K49R	4_1	1, 2	1, 2, 4, 5, 6	1.5	19.6/20.6	0.327	3.20	2z6r
E54H	4_1	1, 3	1, 3	1.9	20.2/21.9	0.096	0.34	2dxv
E54K	4_1	1, 3	3	1.8	19.5/20.3	0.101	0.67	2dxw
E54R	4_1	1, 2, 3	2, 3	1.8	19.9/21.6	0.128	0.79	2e7r
L65A	2	−2, 4	−2, 4	2.2	19.8/22.8	0.140	0.55	2dv5
L65Q	2	1	−2	2.2	19.7/22.5	0.108	0.24	2dv4
N69K	2	1, 2, −4	1, 2, 6	1.8	19.8/21.3	0.117	0.47	2ehc
D79E	4_1	1, 2, −4	1, 2	1.9	19.7/21.2	0.122	0.78	2e07
E140K	4_1, 2	1, 3	1, 3	2.0	20.3/23.1	0.120	0.47	2e08
E140N	4_1, 2	3, 4	3, 4	1.9	20.1/22.3	0.122	0.00	2egb
E140R	4_1, 2	1, 2, 3	1, 3	2.0	20.3/22.8	0.138	0.80	2e16
N142E	4_1, 2_1, 2	1, 2, −4	1, 2, −4	1.75	19.9/21.2	0.121	0.66	2dxx
T146R	4_1, 2_1, 2	1, 2	1, 2, 5, 6	1.6	18.5/19.9	0.299	3.46	2ehl
E171K	2	1, 3	1, 3, −4	1.8	19.9/21.3	0.119	0.00	2egl
E171R	2	1, 3	3, −5	2.2	20.6/23.8	0.158	0.48	2dsi
R173A	4_1, 2	4	4	1.9	19.2/20.9	0.125	0.71	2e17
R173N	4_1, 2	4	4	1.8	19.7/21.1	0.129	0.73	2e15
K187R	2_1	1, 2	−1, −5	2.3	21.5/24.1	0.177	0.54	2dv7
L261M	4_1, 2	2	2	1.9	22.1/24.2	0.124	0.43	2egs

† Contact modifications were classified using the following criteria. A minus sign denotes a reverse effect. 1, increased polar interactions. 2, increased nonpolar interactions. 3, resolved electrostatic repulsions. 4, reduced surface entropy; 5, induced favourable packing rearrangement in other regions; 6, binding ligands at packing interface.

Proteins were eluted with a linear gradient of 0–0.3 *M* NaCl in buffer *A*. The fractions containing mutant *Ph*DS were desalted using a HiPrep 26/10 desalting column with buffer *A* and subjected to a Resource Q column (Amersham Biosciences) equilibrated with buffer *A*. Proteins were eluted with a linear gradient of 0–0.3 *M* NaCl in buffer *A*. The fractions containing mutant *Ph*DS were buffer-exchanged to 10 m*M* phosphate–NaOH pH 7.0 using a HiPrep 26/10 desalting column and applied onto a Bio-Scale CHT-20-I column (Bio-Rad) equilibrated with the same buffer. Proteins were eluted with a linear gradient of 10–250 m*M* phosphate–NaOH pH 7.0. The fractions containing mutant *Ph*DS were pooled, concentrated by ultrafiltration using a Vivaspin concentrator (Vivascience; 10 kDa cutoff) and loaded onto a HiLoad 26/60 Superdex 200pg column (Amersham Biosciences) equilibrated with buffer *A* containing 0.2 *M* NaCl. The purified protein showed a single band on SDS–PAGE. The purified mutant proteins were concentrated to 25–30 mg ml^{-1} using a Vivaspin concentrator (10 kDa cutoff) and stored at 277 K.

2.2. Crystallization and data collection

Crystallization of all *Ph*DS mutants was performed by the oil-microbatch method (Chayen *et al.*, 1990) using the same conditions as used for wild-type *Ph*DS. The crystallization drop was prepared by mixing equal volumes (1.0 µl) of precipitant solution (1.8 *M* ammonium sulfate, 0.01 *M* cobalt chloride, 0.1 *M* MES–NaOH pH 6.5) and protein solution (25–30 mg ml^{-1} *Ph*DS, 0.2 *M* sodium chloride, 20 m*M* Tris–HCl pH 8.0). The crystallization drop in a well of a Nunc HLA plate (Nalge Nunc International) was overlaid with a 3:7 mixture of silicon and paraffin oils, allowing slow evaporation of water in the drop, and stored at 295 K. X-ray diffraction data were collected on a Rigaku R-AXIS V image-plate detector using synchrotron radiation on beamline BL26B1 of SPring-8, Japan (Ueno *et al.*, 2006). For data collection under cryogenic conditions, crystals were soaked for a few minutes in a cryoprotectant solution containing 25%(*v*/*v*) glycerol, 1.8 *M* ammonium sulfate, 0.01 *M* cobalt chloride and 0.1 *M* MES–NaOH pH 6.5. Data were processed and scaled using *HKL*-2000 (Otwinowski & Minor, 1997). Although we did not adopt a strict cutoff criterion to define the resolution limit, it was considered that the $\langle I/\sigma(I)\rangle$ and R_{merge} values in the outmost shell are around 6 and 0.4, respectively. The actual distribution of these values in the outermost shell was 3.4–8.3 for $\langle I/\sigma(I)\rangle$ and 0.27–0.50 for R_{merge}. Statistics of the crystallographic analysis are shown in Table 2 and Supplementary Table 1[1].

2.3. Structure refinement

The structure of each mutant was solved by the molecular-replacement method using the program *MOLREP* (Vagin & Teplyakov, 1997) from the *CCP*4 program suite (Collaborative Computational Project, Number 4, 1994) using wild-type *Ph*DS as the search model (PDB code 1wng). Refinement was carried out using the program *CNS* (Brünger *et al.*, 1998). The structure was visualized and modified using the program *Coot* (Emsley & Cowtan, 2004). The stereochemistry of the models was evaluated with the program *PROCHECK* (Laskowski *et*

[1] Supplementary material has been deposited in the IUCr electronic archive (Reference: MH5014). Services for accessing this material are described at the back of the journal.

Table 2
Data-collection and refinement statistics for selected *Ph*DS mutants.

Values in parentheses are for the highest resolution shell.

	K49R	N69K	D79E	N142E	T146R	E171K
Data collection						
X-ray wavelength (Å)	1.0	1.0	1.0	1.0	1.0	1.0
Space group	$P4_12_12$	$P4_12_12$	$P4_12_12$	$P4_12_12$	$P4_12_12$	$P4_12_12$
Unit-cell parameters						
a, b (Å)	104.5	105.0	105.1	105.2	104.4	104.8
c (Å)	137.5	136.7	136.8	137.0	138.4	137.3
Resolution range (Å)	30.0–1.50 (1.55–1.50)	30.0–1.80 (1.86–1.80)	30.0–1.90 (1.97–1.90)	30.0–1.75 (1.81–1.75)	30.0–1.60 (1.66–1.60)	30.0–1.80 (1.86–1.80)
Unique reflections	121413 (12000)	71341 (7002)	60992 (5985)	77854 (7680)	101013 (9991)	71181 (7009)
Redundancy	10.7 (10.6)	10.9 (11.0)	10.9 (11.2)	10.6 (10.6)	9.0 (6.2)	9.9 (9.8)
Completeness (%)	99.9 (100)	100 (99.8)	99.9 (100)	99.9 (99.9)	100 (100)	99.8 (100)
$\langle I/\sigma(I)\rangle$	13.9 (5.65)	17.1 (6.26)	16.5 (7.09)	15.7 (6.16)	15.1 (5.44)	19.9 (7.32)
$R_{\rm merge}$† (%)	8.3 (39.9)	7.3 (41.6)	8.0 (36.5)	14.7 (40.8)	6.1 (31.7)	6.4 (32.4)
Refinement						
Resolution (Å)	30.0–1.50	30.0–1.80	30.0–1.90	30.0–1.75	30.0–1.60	30.0–1.80
No. of atoms	5110	4839	4768	4860	5003	4940
$R_{\rm work}/R_{\rm free}$‡ (%)	19.6/20.6	19.8/21.3	19.7/21.2	19.1/21.2	18.5/19.9	19.9/21.3
Estimated coordinate error§ (Å)	0.18	0.20	0.22	0.21	0.17	0.21
R.m.s.d. bonds (Å)	0.006	0.006	0.006	0.006	0.006	0.006
R.m.s.d. angles (°)	1.4	1.4	1.3	1.4	1.4	1.3
Ramachandran plot						
Most favoured region (%)	93.5	92.7	92.7	93.1	92.7	92.5
Additional allowed region (%)	6.5	7.3	7.3	6.9	7.3	7.5

† $R_{\rm merge} = \sum_{hkl}\sum_i |I_i(hkl) - \langle I(hkl)\rangle|/\sum_{hkl}\sum_i I_i(hkl)$, where $I_i(hkl)$ and $\langle I(hkl)\rangle$ are the observed intensity of measurement i and the mean intensity of the reflection with indices hkl, respectively. ‡ $R_{\rm work} = \sum ||F_{\rm o}| - |F_{\rm c}||/\sum |F_{\rm o}|$, where $F_{\rm o}$ and $F_{\rm c}$ are the observed and calculated native structure factors, repectively. $R_{\rm free}$ is the same as R but calculated using 5% of the total reflections which were chosen randomly and omitted from the refinement. § The coordinate error was estimated using the Luzzati plot (Luzzati, 1952).

al., 1993) and the acceptable quality of each model was confirmed (Table 1). The statistics of the refinement are summarized in Table 2 and Supplementary Table 1. The structural differences between the wild-type and mutant structures were calculated using the program *LSQKAB* (Kabsch, 1976) from the *CCP*4 suite. Buried surface areas were calculated using the program *SURFACE* (Lee & Richards, 1971) from the *CCP*4 suite.

3. Results

3.1. Systematic design of mutational experiment

The wild-type crystal structure of *Ph*DS belongs to space group $P4_12_12$ and its crystallographic asymmetric unit contains a biological dimer with local pseudo-twofold symmetry (Kishishita *et al.*, 2008). The monomeric protomer of this enzyme is composed of two α/β domains and the interdomain pocket constitutes the catalytic active site. In the *Ph*DS dimer with two catalytic pockets only subunit *A* binds a molecule of the reaction product *S*-adenosyl-L-homocysteine within the pocket; the other subunit *B* is in an apo form. In the *Ph*DS crystal, the crystal packing is mediated by intermolecular interactions between the asymmetric unit dimer and five adjacent crystallographic symmetry-related dimers (Fig. 1*a*): 4_1 screw $-y + 3/2, x + 1/2, z + 1/4$ (sym1) and $y - 1/2, -x + 3/2, z - 1/4$ (sym2), 2_1 screw $-x + 1/2, y - 1/2, -z + 5/4$ (sym3) and $-x + 1/2, y + 1/2, -z + 5/4$ (sym5), and twofold $y - 1, x + 1, -z + 1$ (sym4). The accessible surface area (ASA) of the wild-type *Ph*DS dimer is calculated as 21 180 Å^2. The buried ASAs at the three types of crystal contacts are 843 Å^2 (4_1 screw), 461 Å^2 (2_1 screw) and 654 Å^2 (twofold) per dimer, indicating that 18.5% of the total ASA of the *Ph*DS dimer is buried by crystal packing.

In order to elucidate the relationship between the intermolecular interactions in the crystal packing and the X-ray diffraction quality, *i.e.* the resolution, of protein crystals, a systematic site-directed mutagenesis experiment has been performed on the crystal-packing residues. The crystal-packing residues to be mutated were selected so as to cover all three types of crystal-contact patches, except for residues that were concomitantly involved in dimerization. All mutants were designed and prepared based on a modelling study using the wild-type crystal structure of *Ph*DS. The putative mutants were generated on a graphics system using the program *QUANTA* (Accelrys Inc.) in order to select candidates that should provide better packing interactions without steric clashes (expected contact modifications in Table 1). The following four factors were considered as evaluation criteria for crystal packing: increased polar interactions, increased nonpolar interactions, resolved electronic repulsions and reduced conformational entropy. Because increased interactions and reduced conformational entropy tend to counteract each other, some mutants have a combination of factors with positive and negative effects on crystal packing. In order to compare the crystal structures exactly, the overall crystal-packing mode in the wild-type crystal should be essentially retained in all the mutant crystals. Therefore, all the mutants were crystallized using the same conditions as used for the wild-type protein and no further optimization of the crystal-

lization conditions was performed. We succeeded in obtaining crystals of 21 mutants and determined all their crystal structures, which were nearly isomorphous to that of the wild-type crystal (Table 2 and Supplementary Table 1). After structural determination, the mutants were evaluated according to the following criteria (Table 1). The results of contact modification were evaluated as a combination of six factors contributing to better crystal packing: increased polar interactions, increased nonpolar interactions, resolved electrostatic repulsions, reduced surface entropy, induced favourable packing rearrangement in other regions and binding ligands at the packing interface. The resolution of the mutant crystal was evaluated as an index of X-ray diffraction quality and the overall structural change of the mutant dimer compared with the wild-type dimer, which is resolved into two factors: the root-mean-square deviation (r.m.s.d.) from a C^{α} superposition as an index of the local deformation of the dimer and the rigid-body rotation of the dimer in the asymmetric unit. From the 21 mutants, the following six mutants will be focused on and discussed in detail (Fig. 1*b* and Table 2): three mutants that provided results in good agreement with the designed putative structure (D79E, N142E and E171K) and three mutants that provided unexpected successful results (K49R, N69K and T146R).

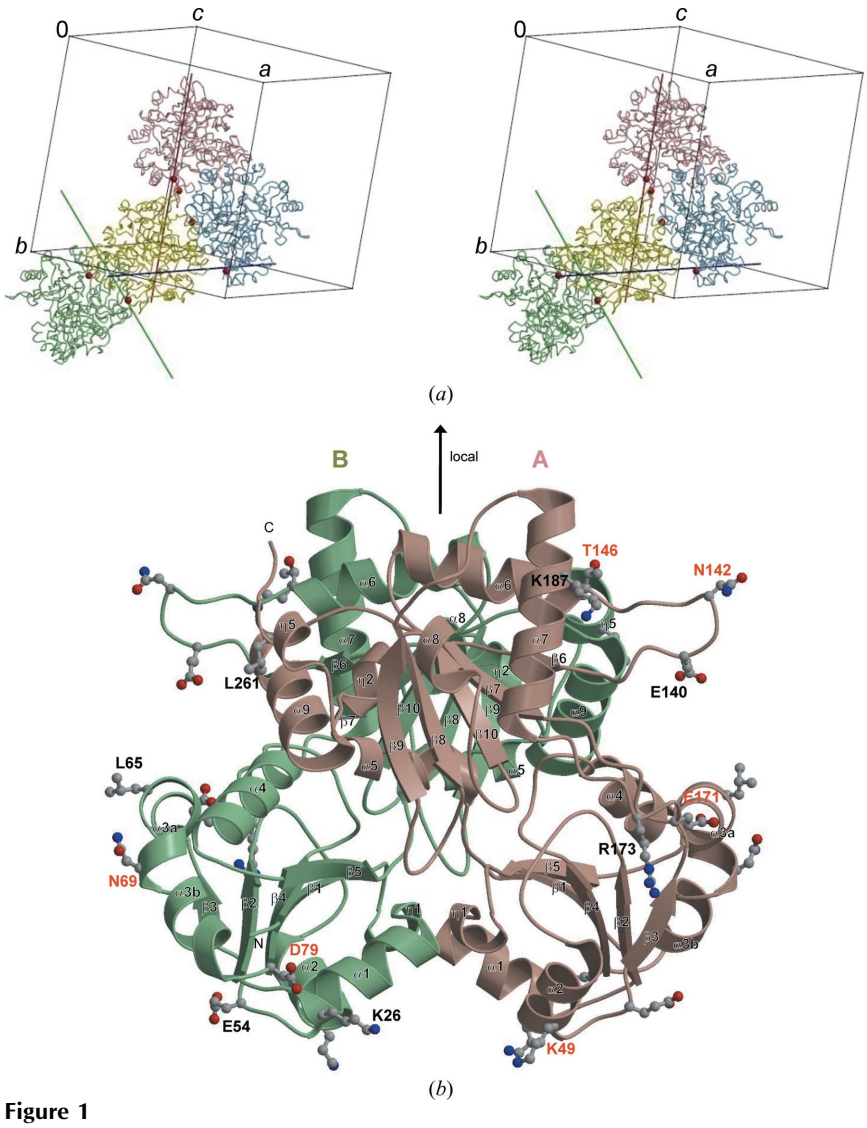

Figure 1
Wild-type structure of *Ph*DS. (*a*) Crystal packing around the asymmetric unit dimer (shown in yellow). The neighbouring dimers coloured blue, pink and green correspond to those related by 4_1 screw (sym1), 2_1 screw (sym3) and twofold (sym4) crystallographic symmetry, respectively. The other symmetry-related dimers sym2 and sym5 are omitted for clarity. The crystallographic symmetry axis for each neighbouring dimer is depicted by a bar with the corresponding colour code. The locations of some of the residues to be mutated are indicated by red spheres. (*b*) Overall ribbon representation of the wild-type *Ph*DS dimer with secondary-structure assignments. The local twofold axis of the dimer is indicated by an arrow. The residues to be mutated are depicted as ball-and-stick models and labelled. The residues selected for detailed discussion in this report are labelled in red. All figures except Figs. 5 and 8 were produced using the programs *MOLSCRIPT* (Kraulis, 1991) and *Raster3D* (Merritt & Murphy, 1994).

3.2. Mutant proteins providing expected packing interactions

3.2.1. D79E mutant. Asp79 is located at the N-terminus of strand β4 and is involved in an intermolecular crystal contact related by the 4_1 screw symmetry sym2. In the wild-type structure, Asp79 in the *A* subunit of the asymmetric unit dimer, notated as Asp79(*A*), forms a hydrogen bond to a water molecule Wat610 and Wat610 forms a hydrogen bond to Arg262 in the sym2-related subunit *B* of another dimer, notated as Arg262(sym2*B*) (Fig. 2*a*). These water-mediated hydrogen bonds, notated as Asp79(*A*) $O^{\delta1}$–Wat610, Wat610–Arg262(sym2*B*) $N^{\eta1}$ and Wat610–Arg262(sym2*B*) $N^{\eta2}$, have interatomic distances of 2.70, 2.96 and 2.66 Å, respectively. The other Asp79 in subunit *B*, notated as Asp79(*B*), is free from crystal contacts since it is located in a solvent-exposed environment in the crystal. We designed the D79E mutant so that the substitution by the longer side chain might provide more intimate intermolecular interactions, although it may also increase the conformational entropy. The D79E mutant yielded crystals with a slightly improved resolution of 1.9 Å (Table 1). In subunit *A* of the mutant structure, Glu79(*A*) $O^{\varepsilon2}$ forms a charged hydrogen bond to Arg262(sym2*B*) $N^{\eta1}$ with an interatomic distance of 2.5 Å (Fig. 2*b*). Additionally, the intermolecular nonpolar interactions between the side chains of Glu79(*A*) and Arg258(sym2*B*) are more intimate when compared with those in the wild-type structure. Notably, although it is not directly related to the crystal contacts, a new intramolecular hydrogen bond Glu79(*B*) $O^{\varepsilon1}$–Tyr4(*B*) O^{η} with a distance of 3.12 Å is observed in subunit *B*, indicating

that the increase in conformational entropy arising from the small-to-large mutation is compensated for by this new intramolecular interaction. The C^{α} superposition between the wild-type and the D79E mutant structures yields small values for both the local deformation (0.122 Å r.m.s.d.) and the rigid-body rotation (0.78°) of the *Ph*DS dimer, suggesting limited structural changes arising from this mutation.

3.2.2. N142E mutant. Asn142 is located at the tip of the $\beta6$–$\alpha6$ hairpin loop which protrudes from the molecular surface of the *Ph*DS dimer and is involved in a major intermolecular crystal contact related by the 2_1 screw symmetry sym3/sym5 as well as a minor contact related by the 4_1 screw symmetry sym1 and the twofold symmetry sym4. In the crystal lattice, each hairpin loop in the *A* or *B* subunit of the asymmetric unit dimer is in contact with an equivalent loop on the subunit sym3*B* or sym5*A* of the neighbouring dimer, respectively, *via* a few direct polar interactions and many nonpolar interactions. In the two hairpin loops of the asymmetric unit dimer, each Asn142 makes a hydrogen bond to a water molecule: Asn142(*A*) $O^{\delta1}$–Wat48 and Asn142(*B*) $N^{\delta2}$–Wat75, with interatomic distances of 2.45 and 2.81 Å, respectively (Fig. 3*a*). These water molecules make weak water-mediated indirect intermolecular interactions with the neighbouring dimer subunits sym3*B* and sym5*A*: Wat48 is located in the vicinity of Thr146(sym3*B*) N and Ser147(sym3*B*) N with distances of 3.43 and 3.48 Å, respectively, and Wat75 is located within hydrogen-bonding distances of Thr146(sym5*A*) N (3.22 Å) and Ser147(sym5*A*) N (3.13 Å). Additionally, each side chain of Trp143, which is the residue next to the mutation site, in the *A* or *B* subunit of the asymmetric unit dimer makes several nonpolar interactions with the subunit sym1*B* or sym4*B* of a different neighbouring dimer, respectively. The N142E mutation was designed with the aim of increasing the crystal-packing interactions by the substitution by a longer side chain with negative charge which might be helpful in forming direct hydrogen bonds with the main-chain N atoms as well as in providing more intimate nonpolar packing interactions. The N142E mutant yielded crystals with a markedly improved resolution of 1.75 Å (Table 1). In both of the subunits of the asymmetric unit dimer the mutated residue Glu142 makes a hydrogen bond to the main-chain N atom of Thr146 as expected: Glu142(*A*) $O^{\varepsilon2}$–Thr146(sym3*B*) N and Glu142(*B*) $O^{\varepsilon2}$–Thr146(sym5*A*) N with distances of 2.89 and 2.78 Å, respectively (Fig. 3*b*). Another large difference is observed in the side-chain conformation of Trp143, in which χ_1/χ_2 rotations of the side chains of 120° in χ_1 and 180° in χ_2 for Trp143(*A*) and 180° in χ_2 for Trp143(*B*) induce novel intermolecular nonpolar interactions Trp143(*A*)–Trp143(sym3*B*) and Trp143(*B*)–Trp143(sym5*A*) as well as a novel intermolecular hydrogen bond Trp143(*A*) $N^{\varepsilon1}$–Val57(sym1*B*) O with a distance of 2.97 Å. Additionally, a molecule of 2-(*N*-morpholino)ethanesulfonate (MES), which is derived from the crystallization reagent, is found in the catalytic pocket of subunit *B*, which is occupied by water molecules in the wild-type structure. A C^{α} superposition between the wild-type and the N142E mutant structure yields small values of both the local deformation (0.121 Å r.m.s.d.) and the rigid-body rotation (0.66°) of the *Ph*DS dimer. Furthermore, the r.m.s.d. value is reduced to 0.104 Å if only the *B* subunits with MES binding are compared. These facts suggest limited structural changes arising from this mutation and no MES-induced conformational changes. It is probable that the N142E mutation has only provided more intimate crystal-packing interactions in the vicinity of the mutation site as expected, without further mutation-induced structural changes in other regions, thereby successfully improving the diffraction quality of the *Ph*DS crystals.

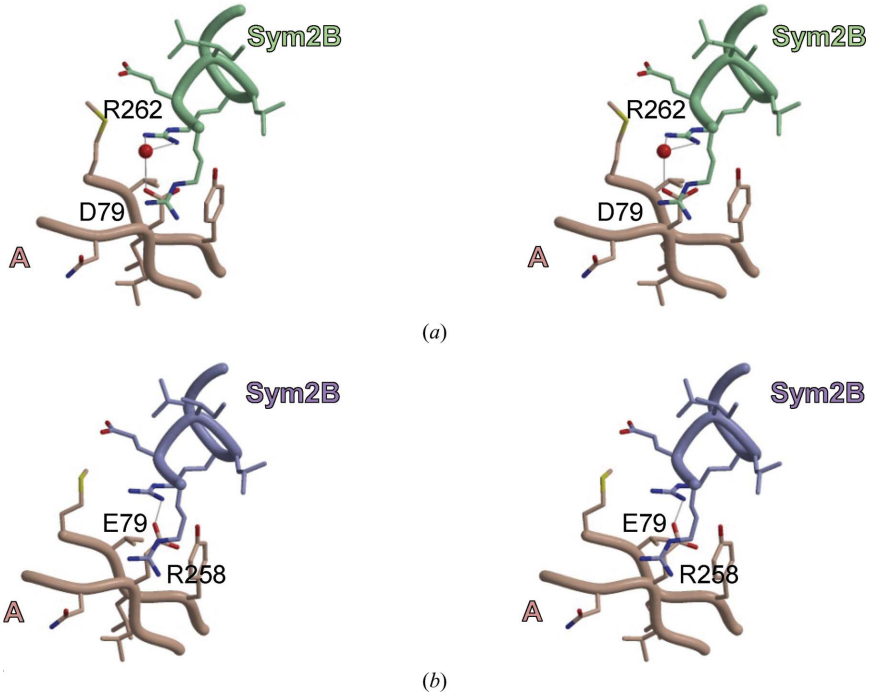

Figure 2
Stereoview of crystal packing around the 79th residue. The side chains of important residues are depicted as liquorice models. Hydrogen bonds are indicated by thin lines. (*a*) Wild type. A red sphere represents a water molecule. (*b*) D79E mutant.

3.2.3. E171K mutant. Glu171 is located at the tip of the $\beta7$–$\alpha7$ hairpin loop. In the wild-type structure, Glu171(*B*) of the asymmetric unit dimer is involved in an intermolecular crystal contact with a neighbouring dimer related by twofold symmetry sym4, whereas Glu171(*A*) is exposed to solvent and free from crystal contacts. Notably, an electrostatic repulsion is observed between the side chains of Glu171(*B*) and Glu140(sym4*B*) in the wild type (Fig. 4*a*). In order to resolve the electrostatic repulsion and to make a new intermolecular polar interaction, the E171K mutation was designed. The E171K mutant yielded crystals with an improved resolution of 1.8 Å (Table 1). In the E171K crystal, the side chain of Lys171(*B*) makes the expected

intermolecular hydrogen bond Lys171(B) N$^{\zeta}$–Glu140(sym4B) O$^{\varepsilon2}$ with a distance of 3.14 Å (Fig. 4b). However, the side chain of Lys171(A) is found to be disordered; electron densities for the C$^{\varepsilon}$ and N$^{\zeta}$ atoms of Lys171(A) are missing, whereas the corresponding side chain is ordered in the wild-type crystal. A C$^{\alpha}$ superposition between the wild-type and the E171K mutant dimers gives an r.m.s.d. value of 0.119 Å and a rigid-body rotation of 0°, indicating no significant overall structural changes arising from this mutation. It is probable that the E171K mutation provides better intermolecular contacts as expected in the vicinity of the mutation site, thereby resulting in better diffraction-quality crystals, even though the disordered side chain of Glu171 in solution would act as a negative factor since it gives an unfavourable entropic penalty upon crystallization. We also examined the E171R mutation, aiming for the same effect. However, the side chain of Arg171(B) did not show the expected intermolecular interaction with Glu140(B) and resulted in crystals with a worse resolution of 2.2 Å.

3.3. Mutant proteins providing unexpected packing interactions

3.3.1. K49R mutant. Lys49 is located on the solvent-exposed side of the α2 helix. In the wild-type structure, Lys49(B) of the asymmetric unit dimer is involved in an intermolecular crystal contact with the neighbouring dimer related by the 4_1 screw symmetry sym2, whereas Lys49(A) is free from crystal contacts. Electron densities corresponding to the side chains of both Lys49(A) and Lys49(B) are not clear in the wild-type crystal (Fig. 5a); the average B factors of the side-chain atoms are 49.6 and 46.4 Å^2, respectively. Lys49(B) in the asymmetric unit dimer forms water-mediated hydrogen bonds to the sym2A subunit of another neighbouring dimer; the hydrogen bonds Lys49(B) N$^{\zeta}$–Wat573, Wat573–Thr93(sym2A) O$^{\gamma1}$ and Wat573–Glu64(sym2A) O$^{\varepsilon1}$ have interatomic distances of 2.84, 2.80 and 2.89 Å, respectively (Fig. 6a). The K49R mutation was designed with the aim of forming direct hydrogen bonds to Glu64(sym2A) as well as extending nonpolar packing interactions and yielded crystals with an outstandingly improved resolution of 1.5 Å (Fig. 5b and Table 1). In contrast to the flexible features of Lys49(A) in the wild-type crystal, the side chain of the mutated residue Arg49(A) is anchored to the main body of subunit A by indirect hydrogen bonds mediated by a sulfate ion Sul1305(A) in the mutant crystal; the hydrogen bonds Arg49(A) N$^{\eta1}$–Sul1305(A) O^{1}, Arg49(A) N$^{\eta2}$–Sul1305(A) O^{4} and Sul1305(A) O^{4}–Thr43(A) O$^{\gamma1}$ have distances of 2.94, 2.88 and 2.77 Å, respectively. Thus, in the K49R mutant crystal electron densities corresponding to the side chains of both Arg49(A) and Arg49(B) are very clear; the average B factors of the side-chain atoms are 22.8 and 16.0 Å^2, respectively. Since this mutation-induced ordering of the side chain implies surface-entropy reduction upon crystallization, the K49R mutation would be thermodynamically favourable for crystallization, even though it is not a standard substitution in the SER

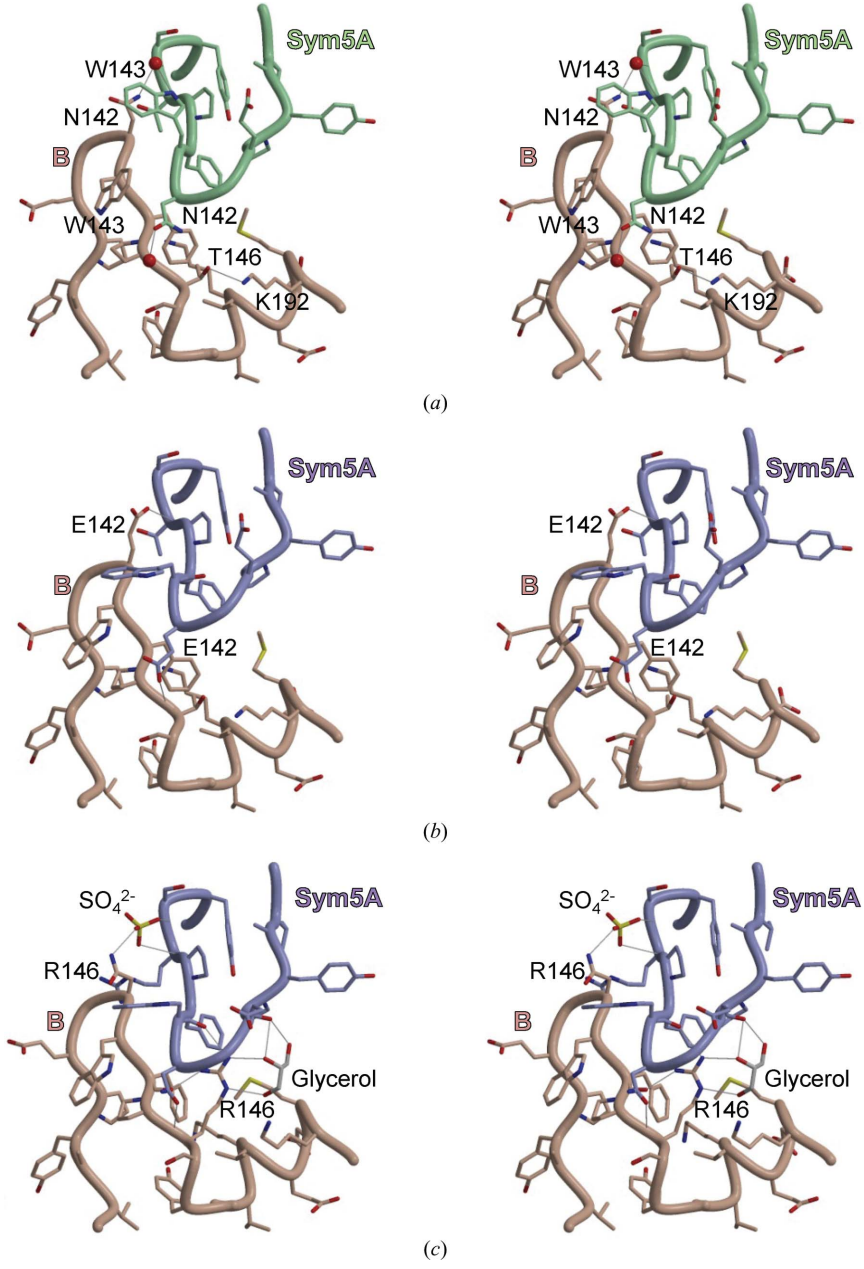

Figure 3
Stereoview of crystal packing around the β6–α6 hairpin loop. The side chains of important residues are depicted as liquorice models. Hydrogen bonds are indicated by thin lines. (*a*) Wild type. A red sphere represents a water molecule. (*b*) N142E mutant. (*c*) T146R mutant. Bound sulfate ion and glycerol are depicted as liquorice models.

method. Polar and nonpolar intermolecular interactions at the mutated residue Arg49(*B*) are dramatically increased by an unexpected rearrangement of the interface (Fig. 6*b*). Firstly, the mutated residue Arg49(*B*) does not form the expected direct hydrogen bond to Glu64(sym2*A*) but forms a van der Waals stacking of side chains in which the side chain of Arg49(*B*) is sandwiched between the carboxylate planes of Glu64(sym2*A*) and Glu96(sym2*A*). A new direct hydrogen bond is formed between Arg49(*B*) N^{ε} and Thr93(sym2*A*) $O^{\gamma1}$ with a distance of 2.85 Å. Additionally, water-mediated hydrogen bonds further stabilize the packing interaction; the hydrogen bonds Arg49(*B*) $N^{\eta2}$–Wat1508(sym2*A*), Wat1508(sym2*A*)–Thr93(sym2*A*) $O^{\gamma1}$ and Wat1508(sym2*A*)–His94(sym2*A*) $N^{\delta1}$ have distances of 3.00, 2.88 and 2.82 Å, respectively. Furthermore, a bridging glycerol molecule Gol1403(sym2*A*) is identified with clear electron density. The side chain of Arg49(*B*) forms glycerol-mediated hydrogen bonds with the sym2*A* subunit; the hydrogen bonds Arg49(*B*) $N^{\eta1}$–Gol1403(sym2*A*) O^3, Arg49(*B*) $N^{\eta2}$–Gol1403(sym2*A*) O^3, Gol1403(sym2*A*) O^1–Glu68(sym2*A*) $O^{\varepsilon1}$ and Gol1403(sym2*A*) O^2–Arg100(sym2*A*) N^{ε} have distances of 2.77, 2.68, 2.37 and 3.00 Å, respectively. A C^{α} superposition between the wild-type and the K49R mutant structures yields very large values for both the local deformation (0.327 Å r.m.s.d.) and rigid-body rotation (3.20°) of the *Ph*DS dimer, suggesting large mutation-induced conformational changes. This rigid-body relocation of the dimer in the asymmetric unit seems to induce large indirect local shifts of dimer atoms in regions far from the mutation site, especially in the $\beta6$–$\alpha6$ hairpin loop, which shows marked C^{α} shifts of more than 1 Å. Major mutation-induced local structural changes in residues distant from the mutation site include (i) Asn142(*A*), which is 21.1 Å away ($C^{\alpha}-C^{\alpha}$) from Arg49(sym1*B*), which has a conformational change of its side chain to form a direct packing hydrogen bond Asn142(*A*) $N^{\delta2}$–Asp62(sym1*B*) $O^{\delta2}$ with a distance of 2.93 Å and sulfate-mediated packing hydrogen bonds Asn142(*A*) $N^{\delta2}$–Sul1304(*A*) O^4, Sul1304(*A*) O^2–Thr146(sym3*B*) N, Sul1304(*A*) O^3–Ser147(sym3*B*) N and Sul1304(*A*) O^3–Ser147(sym3*B*) O^{γ} with distances of 2.96, 2.96, 3.02 and 2.79 Å, respectively; (ii) Lys241(*A*), which is 36.5 Å away from Arg49(sym4*B*) and has a conformational change of its side chain to form a new packing hydrogen bond Lys241(*A*) N^{ζ}–Asn69(sym4*B*) $O^{\delta1}$ with a distance of 3.02 Å; (iii) Glu68(*B*), which is 27.1 Å away from Arg49(*A*) and has a mutation-induced alternate conformation to form a new packing hydrogen bond Glu68(*B*) $O^{\varepsilon2}$–Ile244(sym4*A*) N with a distance of 2.55 Å; (iv) Asn142(*B*) which is 19.8 Å away from Arg49(sym4*B*) and has a translation of the whole residue to form a new packing hydrogen bond Asn142(*B*) N–Glu171(sym4*B*) O with a distance of 2.84 Å; (v) Trp143(*B*), which is 22.1 Å away from Arg49(sym4*B*) and has a 180° rotation of the side-chain χ_2 angle to form new water-mediated intermolecular hydrogen bonds Trp143(*B*) $N^{\varepsilon1}$–Wat1561(sym4*B*) and Wat1561(sym4*B*)–Ser59(sym4*B*) O^{γ} with distances of 2.96 and 2.74 Å, respectively; and (vi) Phe144(*B*), which is 24.1 Å away from Arg49(sym4*B*) and has a conformational change of its side chain to extend nonpolar packing interactions with the side chain of Phe144(sym5*A*). In the K49R mutant crystal, the asymmetric unit dimer has a buried ASA value of 4558 $Å^2$ at the crystal-packing interface, which is clearly larger than the corresponding value of 3916 $Å^2$ in the wild-type crystal, suggesting that the overall packing interactions are indirectly extended by the mutation. These direct and indirect enhancements of intermolecular packing interactions by the K49R mutation are the most likely reason for it providing the best result of 1.5 Å resolution, even though almost none of them could be predicted.

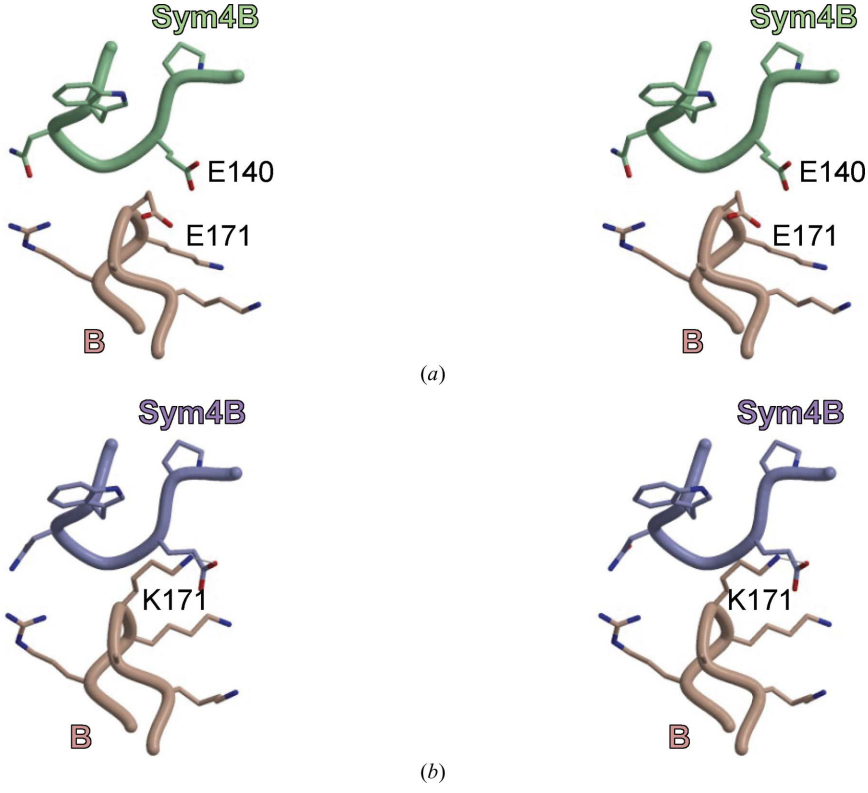

Figure 4
Stereoview of crystal packing around the 171st residue. The side chains of important residues are depicted as liquorice models. Hydrogen bonds are indicated by thin lines. (*a*) Wild type. (*b*) E171K mutant.

3.3.2. N69K mutant. Asn69 is located on the solvent-exposed side of the α3a helix. In the wild-type structure, Asn69(*B*) of the asymmetric unit dimer is involved in an intermolecular crystal contact with the neighbouring dimer related by the twofold symmetry sym4, whereas Asn69(*A*) is free from crystal contacts. The side chain of Asn69(*B*) forms water-mediated hydrogen bonds to the main chain of Leu242(sym4*A*); the hydrogen bonds Asn69(*B*) $O^{\delta1}$–Wat366 and Wat366–Leu242(sym4*A*) O have interatomic distances of 2.44 and 3.16 Å, respectively (Fig. 7*a*). In order to form direct

hydrogen bonds with Leu242(sym4*A*) O as well as to extend nonpolar packing interactions, the N69K mutation was designed, which yielded crystals with an improved resolution of 1.8 Å (Table 1). In the mutant structure, the side chain of Lys69(*B*) does not have the expected interactions but forms a hydrogen bond with a sulfate ion Sul1308(sym4*B*), which makes sulfate-mediated hydrogen bonds with the sym4*B* subunit (Fig. 7*b*); the hydrogen bonds Lys69(*B*) N^{ζ}–Sul1308(sym4*B*) O^{3}, Asn66(*B*) $N^{\delta2}$–Sul1308(sym4*B*) O^{2} and Sul1308(sym4*B*) O^{3}–Lys132(sym4*B*) N^{ζ} have distances of 2.75, 3.13 and 2.75 Å, respectively. It should be noted that some ambiguous electron density is also observed in the wild-type crystal at the position corresponding to the sulfate Sul1308, although it was not modelled in the wild-type structure owing to its ambiguity. Thus, it is possible that higher resolution data of the N69K mutant simply gave more information for this bound sulfate. However, it is also possible that the N69K mutation induced a more defined sulfate–protein interaction at the Sul1308 site, resulting in its clear electron density in the mutant structure. Further analysis is required to clarify this issue. Although not directly related to the crystal contacts, the side chain of the mutated residue Lys69(*A*) is anchored to the main body of subunit *A* by an intramolecular hydrogen bond Lys69(*A*) N^{ζ}–Asn66(*A*) $O^{\delta1}$ with a distance of 2.71 Å. Thus, in the N69K mutant crystal electron densities corresponding to the side chains of both Lys69(*A*) and Lys69(*B*) are visible in spite of the flexible nature of the lysine side chain; the average *B* factors of the side-chain atoms are 44.1 and 35.1 $Å^2$, respectively. This fact suggests that the increase in the conformational entropy from the small-to-large mutation is compensated by the intramolecular anchoring. A C^{α} superposition between the wild-type and the N69K mutant structures yields small values for both the local deformation (0.117 Å r.m.s.d.) and rigid-body rotation (0.47°) of the *Ph*DS dimer, suggesting limited structural changes arising from this mutation. It is likely that the unexpectedly bound sulfate ion increases the intermolecular packing interactions, thereby yielding the improved resolution of the N69K mutant crystals.

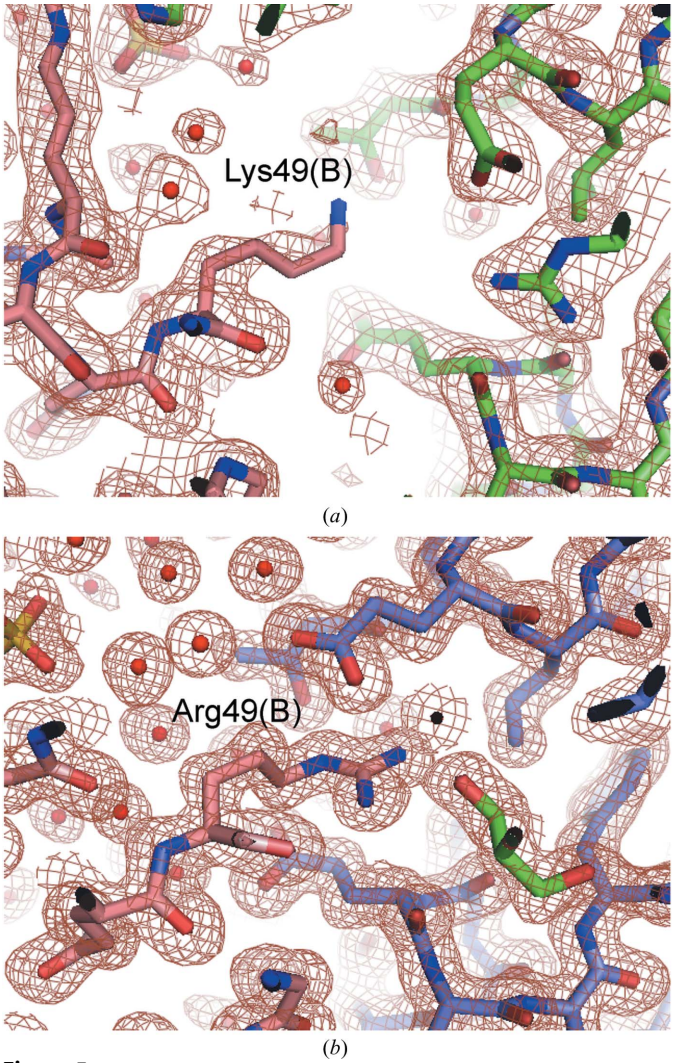

Figure 5
$(2F_o - F_c)$ electron-density map contoured at the 1σ level around the 49th residue. Refined models depicted as liquorice models are superposed. This figure was prepared with *PyMOL* (DeLano, 2002). (*a*) Wild type. (*b*) K49R mutant.

3.3.3. T146R mutant. Thr146 is located at the C-terminus of the $\beta6$–$\alpha6$ hairpin loop and is involved in the major intermolecular crystal contact related by the 2_1 screw symmetry sym3/sym5 as well as the minor contact related by the 4_1 screw symmetry sym1 and the twofold symmetry sym4. The environment of the $\beta6$–$\alpha6$ hairpin loop in the wild-type crystal is as mentioned previously in the N142E mutant. The side chain of Thr146(*A*) is located in the vicinity of Asn142(sym3*B*); the interatomic distance between Thr146(*A*) $O^{\gamma1}$ and Asn142(sym3*B*) $N^{\delta2}$ is 3.27 Å. In contrast, Thr146(*B*) makes an intramolecular hydrogen bond to Lys192(*B*): Thr142(*B*) $O^{\gamma1}$–Lys192(*B*) N^{ζ} with a distance of 3.21 Å (Fig. 3*a*). The T146R mutation was designed with the aim of extending polar and nonpolar interactions with the neighbouring loop, especially the putative hydrogen bonds Arg146(*A*) $N^{\eta1/\eta2}$–Gly141(sym3*B*) O and Arg146(*B*) $N^{\eta1/\eta2}$–Gly141(sym5*A*) O. The T146R mutant yielded crystals with the second best resolution of 1.6 Å (Table 1). In the mutant structure, polar and nonpolar packing interactions are dramatically increased by an unexpected rearrangement of the interface (Fig. 3*c*). In subunit *A* of the asymmetric dimer, the mutated residue Arg146(*A*) does not form the expected direct hydrogen bond to Gly141(sym3*B*) but forms a van der Waals stacking in which the guanidium plane of Arg146(*A*) is aligned with the peptide planes of Gly141(sym3*B*) and Asn142(sym3*B*). Unexpectedly, a bridging sulfate ion Sul1306(sym3*B*) was identified with clear electron density. Arg146(*A*) forms sulfate-mediated hydrogen bonds with the subunits sym3*B* and sym1*B* on different neighbouring dimers: Arg146(*A*) N–Sul1306(sym3*B*) O^{1}, Ser147(*A*) N–Sul1306(sym3*B*) O^{4}, Sul1306(sym3*B*) O^{3}–Asn142(sym3*B*) $N^{\delta2}$, Sul1306(sym3*B*) O^{2}–Arg173(sym1*B*) N^{ε} and Sul1306(sym3*B*) O^{3}–Arg173(sym1*B*) $N^{\eta2}$ with distances of 2.94, 2.98, 2.94, 3.20 and 3.13 Å, respectively. Additionally, large mutation-induced structural differences are observed in the vicinity of the mutation site Arg146(*A*), in which rotations of 120° in χ_1 and 180° in χ_2 of the Trp143(*A*) side chain induce novel inter-

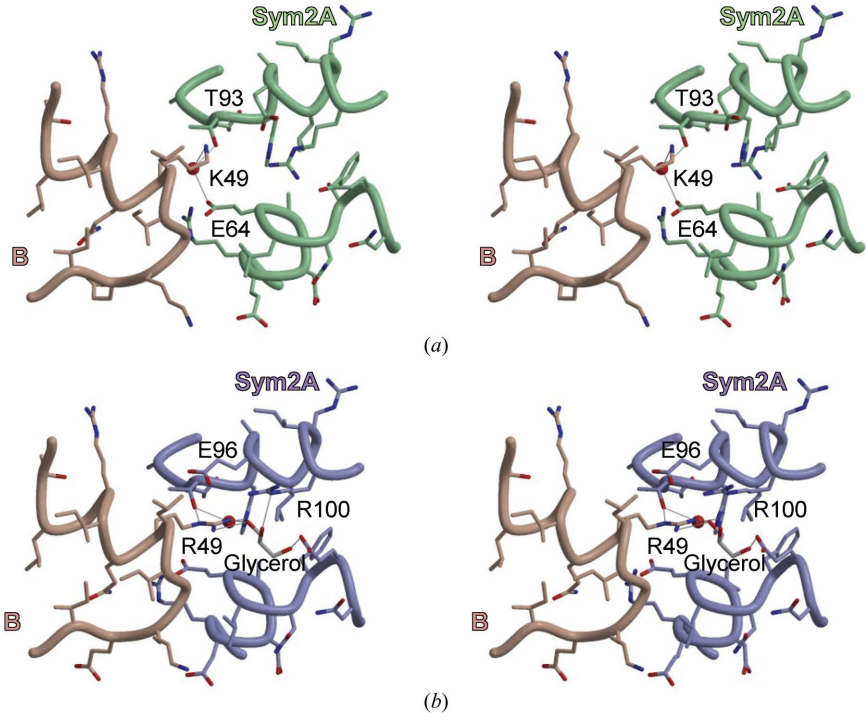

Figure 6
Stereoview of crystal packing around the 49th residue. The side chains of important residues are depicted as liquorice models. Hydrogen bonds are indicated by thin lines. A red sphere represents a water molecule. (*a*) Wild type. (*b*) K49R mutant. Bound glycerol is depicted as a liquorice model.

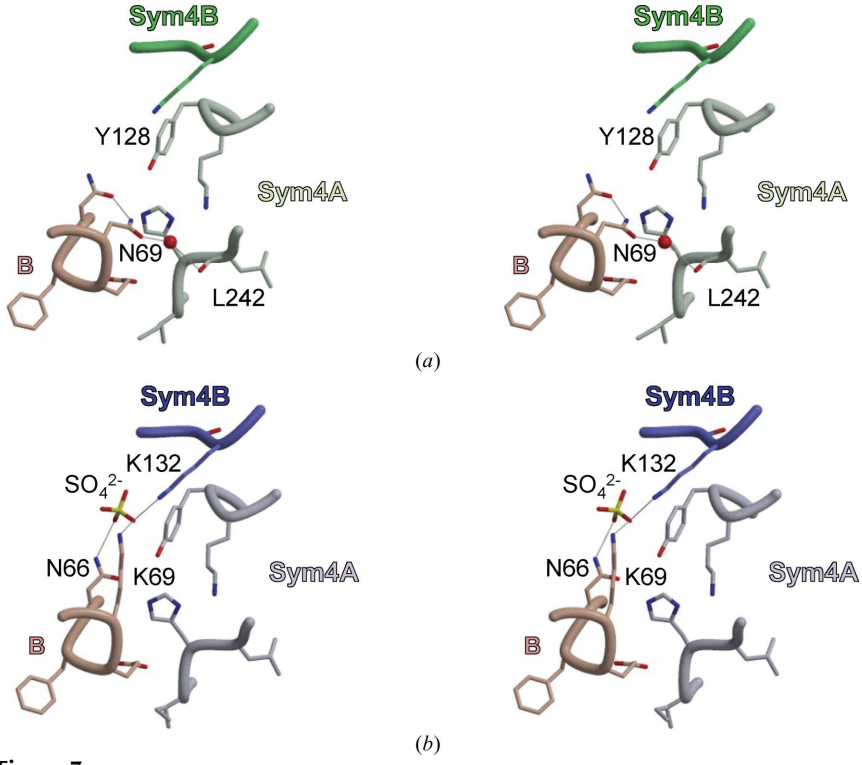

Figure 7
Stereoview of crystal packing around the 69th residue. The side chains of important residues are depicted as liquorice models. Hydrogen bonds are indicated by thin lines. (*a*) Wild type. A red sphere represents a water molecule. (*b*) N69K mutant. Bound sulfate ion is depicted as a liquorice model.

molecular nonpolar interactions Trp143(*A*)–Trp143(sym3*B*) as well as a novel intermolecular hydrogen bond Trp143(*A*) $N^{\varepsilon 1}$–Val57(sym1*B*) O with a distance of 2.96 Å. In subunit *B*, the mutated residue Arg146(*B*) makes two new intermolecular hydrogen bonds to subunit sym5*A*: Arg146(*B*) N–Asn142(sym5*A*) $O^{\delta 1}$ and Arg146(*B*) $N^{\eta 2}$–Trp143(sym5*A*) O with distances of 2.93 and 2.98 Å, respectively. Unexpectedly, a bridging glycerol molecule Gol1405(sym5*A*) was identified with clear electron density. The side chain of Arg146(*B*) forms glycerol-mediated hydrogen bonds to the sym5*A* subunit: Arg146(*B*) N^{ε}–Gol1405(sym5*A*) O^3, Arg146(*B*) $N^{\eta 2}$–Gol1405(sym5*A*) O^2, Gol1405-(sym5*A*) O^1–Pro139(sym5*A*) O and Gol1405-(sym5*A*) O^2–Pro139(sym5*A*) O with distances of 2.91, 2.80, 2.82 and 3.03 Å, respectively. Additionally, large mutation-induced structural differences are observed in the vicinity of the mutation site Arg146(*B*): a 180° χ_2 rotation of the Trp143(*B*) side chain to form the novel intermolecular nonpolar interaction Trp143(*B*)–Trp143(sym5*A*), a large main-chain translation of Asn142(*B*) to form a direct packing hydrogen bond Asn142(*B*) N–Glu171(sym4*B*) O with a distance of 3.02 Å and glycerol-mediated packing hydrogen bonds Asn142(*B*) $O^{\delta 1}$–Gol1403(sym4*B*) O^2, Asn142(*B*) $N^{\delta 2}$–Gol1403(sym4*B*) O^3 and Gol1403(sym4*B*) O^3–Ala170(sym4*B*) O with distances of 2.72, 2.92 and 2.77 Å, respectively. A C^{α} superposition between the wild-type and the T146R mutant structures yields very large values of both the local deformation (0.299 Å r.m.s.d.) and rigid-body rotation (3.46°) of the *Ph*DS dimer, suggesting a large mutation-induced conformational change. This rigid-body relocation of the dimer in the asymmetric unit seems to induce large indirect local shifts of dimer atoms in regions far from the mutation site: Leu65(*A*), which is 27.6 Å away ($C^{\alpha}-C^{\alpha}$) from Arg146(*A*), has 120° rotations of both the χ_1 and χ_2 angles in its side chain owing to novel nonpolar packing interactions with subunit sym1*B* and Arg14(*B*), which is 24.9 Å away from Arg146(sym2*A*) and the side chain of which has common intermolecular hydrogen bonds with the side chain of Glu248(sym2*B*) in both wild-type and T146R mutant crystals, has a conformational change of its side chain owing to the mutation-induced rigid-body shift of the

hydrogen-bonding partner. Additionally, glycerol-mediated packing hydrogen bonds are found at Asn66(*B*), which is 15.1 Å away from Arg146(sym4*B*), although the mutation-induced shift is not so obvious for this change: Asn66(*B*) $O^{\delta1}$–Gol1402(sym4*A*) O^{2} and Gol1402(sym4*A*) O^{2}–Tyr128(sym4*A*) O^{η} with distances of 2.88 and 2.70 Å, respectively. It should be noted that some ambiguous electron densities are also observed in the wild-type crystal at the position corresponding to the glycerol Gol1402, although it was not modelled in the wild-type structure owing to its ambiguity. Thus, it is possible that the higher resolution data of the T146R mutant simply gave more information for this bound glycerol. However, it is also possible that the mutation T146R induced a more defined glycerol–protein interaction at the Gol1402 site, resulting in its clear electron density in the mutant structure. Further analysis is required to clarify this issue. In the T146R mutant crystal, the asymmetric unit dimer has a buried ASA of 4828 $Å^2$ at the crystal-packing interface,

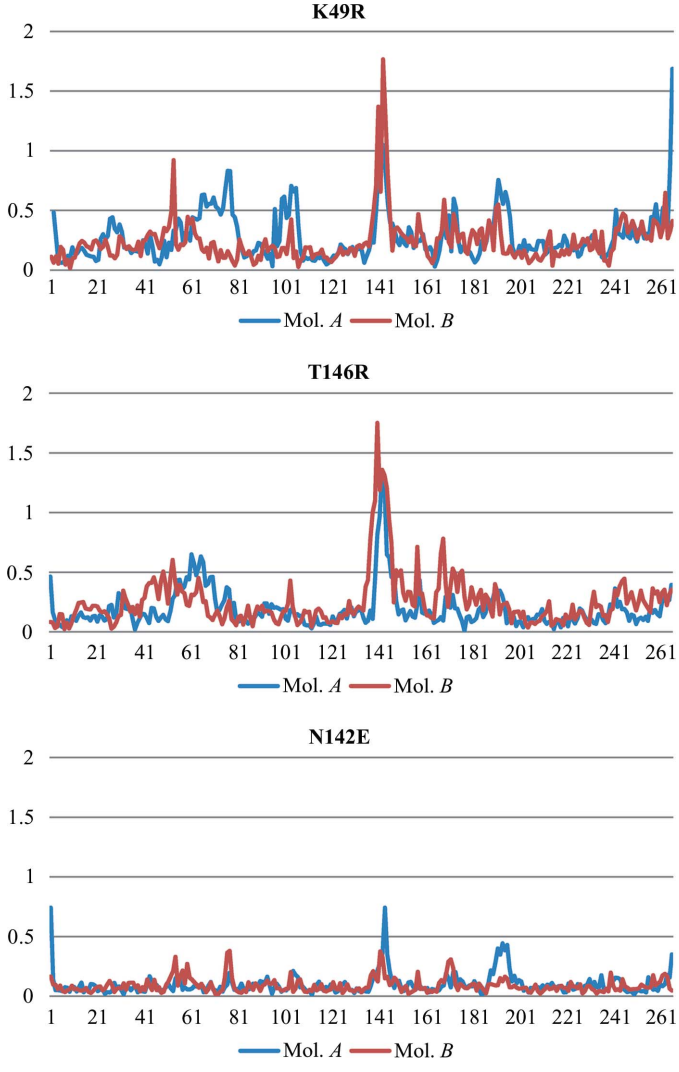

Figure 8
Coordinate deviations from the C^{α} superposition between each mutant structure and the wild-type structure. The coordinate deviations calculated for the selected three mutants (in angstroms) are plotted by residue.

Table 3
Accessible surface area (ASA) analysis of *Ph*DS mutants.

Protein	Resolution (Å)	Dimer ASA ($Å^2$)	Buried ASA by crystal packing ($Å^2$)			
			4_1 screw	2_1 screw	Twofold	Total (ratio)
Wild type	2.1	21180	843	461	654	3916 (18.5%)
K26R	2.0	21009	889	479	651	4038 (19.2%)
K26Y	2.0	21117	868	503	720	4182 (19.8%)
K49R	1.5	21216	1056	534	689	4558 (21.5%)
E54H	1.9	21136	795	446	668	3818 (18.1%)
E54K	1.8	21330	818	459	724	4002 (18.8%)
E54R	1.8	21578	887	524	818	4457 (20.7%)
L65A	2.2	21275	790	473	655	3834 (18.0%)
L65Q	2.2	21157	862	487	716	4129 (19.5%)
N69K	1.8	21257	875	498	780	4306 (20.3%)
D79E	1.9	21404	813	474	785	4144 (19.4%)
E140K	2.0	21326	794	450	679	3847 (18.0%)
E140N	1.9	21415	965	528	812	4610 (21.5%)
E140R	2.0	21442	856	471	666	3985 (18.6%)
N142E	1.75	21103	791	474	695	3920 (18.6%)
T146R	1.6	21181	999	651	764	4828 (22.8%)
E171K	1.8	21585	954	489	877	4640 (21.5%)
E171R	2.2	21199	857	477	782	4231 (20.0%)
R173A	1.9	21235	799	477	714	3980 (18.7%)
R173N	1.8	21162	795	452	688	3870 (18.3%)
K187R	2.3	21271	877	435	751	4126 (19.4%)
L261M	1.9	21362	862	466	760	4175 (19.5%)

which is the largest value in the 21 mutants examined and is clearly larger than the corresponding value of 3916 $Å^2$ in the wild-type crystal (Table 3), suggesting that the overall packing interaction is indirectly extended by the mutation. These direct and indirect enhancements of intermolecular packing interactions by the T146R mutation are the most likely reason for it providing the second best result of 1.6 Å resolution, even though almost all of them could not be predicted.

3.4. Comparison of crystal-packing interaction between mutant proteins

Of the 21 examined mutants of *Ph*DS, the K49R and T146R mutants provided outstandingly improved crystals with respect to the resolution of X-ray diffraction. These two mutants revealed conformational changes that were clearly larger than those of other mutants when each mutant structure was compared with the wild-type structure (Table 1). In order to analyze the distribution of local conformational changes in the mutations, coordinate deviations from the C^{α} superposition between each mutant structure and the wild-type structure were calculated and plotted by residue (Fig. 8 and Supplementary Fig. 1). Notably, in both the K49R and T146R structures marked C^{α} deviations of over 1 Å are observed in the $\beta6$–$\alpha6$ hairpin loop which protrudes from the molecular surface of the *Ph*DS dimer and is involved in the major intermolecular crystal contact related by the 2_1 screw symmetry sym3/sym5 as well as the minor contact related by the 4_1 screw symmetry sym1 and the twofold symmetry sym4. This hairpin loop also tends to show larger local structural changes compared with those in other regions in other mutant structures, indicating that the $\beta6$–$\alpha6$ hairpin loop is a hotspot of structural change upon mutation. Since this hairpin loop protrudes from the dimer surface and mediates many crystal

contacts in the crystal lattice, it is likely that the conformation of the loop tends to greatly be affected by mutation-induced differences in crystal packing. It is probable that a large reconstruction of the packing interface is required to obtain a dramatic improvement in diffraction quality. However, in the case of the N142E mutant, which provided a markedly improved resolution of 1.75 Å, the mutation-induced conformational changes are small except for the residues in the vicinity of the mutation site, indicating that the 1.75 Å resolution is achievable without such a large reconstruction of packing.

To investigate the relationship between the packing-contact area and the crystal quality, the buried ASA value per dimer on crystal packing was calculated for each mutant structure (Table 3). Interestingly, the mutant crystals with larger total buried ASAs at crystal-packing interfaces tend to diffract X-rays to better resolutions. It is likely that an overall increase in the crystal-packing area corresponds to extended polar and nonpolar intermolecular interactions, thereby resulting in a general improvement of diffraction quality. However, the specific crystal-contact patch containing a successful mutation site does not necessarily have a larger buried ASA value. For instance, although the E54R mutant structure at 1.8 Å resolution has the mutation site in the 4_1 screw patch, the buried ASA value increases in the twofold patch rather than in the 4_1 screw patch, indicating that the mutation can affect the packing interactions in regions that are distant from the mutation site. Furthermore, in the N142E mutant structure at 1.75 Å resolution there is no obvious increase in the buried ASA for either each specific contact patch or for the total area, probably because the overall increase in packing area is not sensitive to the quality of interactions such as the geometry of the hydrogen bond and the cooperativity of van der Waals interactions.

3.5. Statistical evaluation

In the present *Ph*DS crystal structures, three characteristics/factors are highlighted as being relevant to the resolution of mutant crystals: the local conformational change of the mutant dimer, represented as the r.m.s.d. value from the C^{α} superposition with the wild-type structure, the rigid-body rotation of the mutant dimer within the asymmetric unit of the crystal and the buried ASA at crystal-contact regions. In order to statistically evaluate the relationship between these factors and the resolution of the crystals, Fisher's exact probability test (Fisher, 1922) has been employed (Table 4). If we classify the *Ph*DS structures into lower or higher resolution groups, combination of these with lower and higher categories of each factor makes a 2×2 contingency table with values a, b, c and d. From this table, the probability of the occurrence of the observed value distribution can be calculated according to the following equation: $P_1 = (a + b)!(c + d)!(a + c)!(b + d)!/(a + b + c + d)!a!b!c!d!$. Using this equation, the probabilities of the other putative value distributions providing further extreme results are also calculated as P_2 to P_n. Fisher showed that we can only deal with cases where the marginal totals ($a + b$, $c + d$, $a + c$ and $b + d$) are the same as in the observed table. The Fisher's exact probability P for the occurrence of observed or further extreme value distributions is given as their summation: $P = P_1 + P_2 + \ldots + P_n$.

Table 4
Fisher's exact probability test to evaluate factor–resolution relationships.

(*a*) R.m.s.d.

	R.m.s.d. < 0.2 Å	R.m.s.d. ≥ 0.2 Å	Total
Resolution > 1.7 Å	19	0	19
Resolution ≤ 1.7 Å	0	2	2
Total	19	2	21

(*b*) Rotation.

	Rotation < 2.0°	Rotation ≥ 2.0°	Total
Resolution > 1.7 Å	19	0	19
Resolution ≤ 1.7 Å	0	2	2
Total	19	2	21

(*c*) Buried ASA.

	Buried ASA < 4300 Å^2	Buried ASA ≥ 4300 Å^2	Total
Resolution > 1.8 Å	13	1	14
Resolution ≤ 1.8 Å	3	5	8
Total	16	6	22

Firstly, the local conformational change is evaluated as the r.m.s.d. value from C^{α} superposition. The threshold levels of resolution and r.m.s.d. were set at 1.7 and 0.2 Å, respectively, because observation suggests that only mutants with exceptionally improved resolution provide exceptionally high r.m.s.d. values. The Fisher's exact probability was calculated as 4.762×10^{-3}. Thus, the very high-resolution (1.7 Å or better) group significantly provides very high r.m.s.d. values (0.2 Å or more) using a significance level of 1%. Secondly, the rigid-body rotation within the asymmetric unit was evaluated. The threshold levels of resolution and rotation were set at 1.7 Å and 2.0°, respectively, because observation suggests that only mutants with exceptionally improved resolution provide exceptionally high values of rotation. The Fisher's exact probability was calculated as 4.762×10^{-3}. Thus, the very high-resolution (1.7 Å or better) group significantly provides very high values of rotation (2.0° or more) using a significance level of 1%. Finally, the buried ASA at crystal contact regions was evaluated. The threshold levels of resolution and buried ASA were set at 1.8 Å and 4300 Å^2, respectively. The Fisher's exact probability was calculated as 0.0109. Thus, the higher resolution (1.8 Å or better) group significantly provides higher values of buried ASA (4300 Å^2 or more) using a significance level of 5%.

4. Discussion

In the present study, we investigated the relationship between the X-ray diffraction quality of protein crystals and the site-directed mutagenesis of crystal-packing residues using the *Ph*DS system. 13 different crystal-packing residues were

selected in order to cover all crystal-contact patches found in the wild-type *Ph*DS crystal. 21 single-mutant proteins were designed, prepared and crystallized under the same crystallization conditions as used for the wild-type protein and yielded nearly isomorphous crystals despite the large variety of mutants. The structural determination of these 21 mutant crystals revealed that the resolution of crystals was successfully improved to 1.8 Å or better in eight mutants (38%). Because the same crystallographer performed all the X-ray diffraction experiments, we could minimize the systematic noise derived from technical differences in crystal manipulation and data collection which may affect the diffraction quality of crystals. Consecutive in-house diffraction experiments by the same person using 13 independent wild-type *Ph*DS crystals with similar crystal sizes revealed a standard error of 0.0231 Å in resolution on the mean value of 2.12 Å, indicating that the reliability of resolution in this experiment is estimated by Student's *t*-distribution as ±0.050 Å with a 95% confidence interval. The reliability of resolution in other experiments would be similar although the standard error of each experiment is not available. An automated evaluation system for the diffraction quality without manual handling of protein crystals is desirable in future in order to improve the efficiency and accuracy of the experiment.

Of the 21 mutants, 14 provided structures that were in good agreement with the designed putative structure: K26R, K26Y, E54H, E54K, E54R, L65A, D79E, E140K, E140N, N142E, E171K, R173A, R173N and L261M, with resolutions of 2.0, 2.0, 1.9, 1.8, 1.8, 2.2, 1.9, 2.0, 1.9, 1.75, 1.8, 1.9, 1.8 and 1.9 Å, respectively. Five of the 14 mutants (36%) successfully provided crystals with a resolution of 1.8 Å or better. Thus, in the *Ph*DS system rational design at crystal contacts can improve the diffraction quality of protein crystals to a resolution of 1.75 Å. The N142E mutation provided the best resolution of 1.75 Å, although such a mutation should be avoided according to SER theory, indicating that a mutation that is unfavourable according to SER is worth trying if it is expected to increase the packing interactions. The L65A mutation, which provided the worst resolution of 2.2 Å, was probably strategically wrong: from the viewpoint of the hydration effect, a leucine-to-alanine mutation at a crystal-contact region is thermodynamically unfavourable, although it is in accordance with the large-to-small substitution of SER. The SER effect and the hydration effect should probably be considered in an integrated manner. The overall structural changes in these 14 mutants are generally small: the average values for the r.m.s.d. from C^{α} superposition and the rigid-body rotation in the asymmetric unit are 0.122 Å and 0.55°, respectively; the largest changes are observed in the K26Y mutant with 0.152 Å r.m.s.d. and 1.07° rotation. If the crystal-packing interactions can be ultimately reduced to the free energy, the crystal-packing free energy of these 14 mutant crystals would be similar because they have essentially the same packing mode. The remaining seven mutants that provide unexpected results can be classified into three categories. The first category contains mutant crystals with outstandingly large overall structural changes in which the r.m.s.d. from C^{α} superposition and the rigid-body rotation in the asymmetric unit are more than 0.2 Å and 2.0°, respectively. Two mutations, K49R and T146R, provided crystals with outstandingly improved resolutions of 1.5 and 1.6 Å, respectively. The statistical relevance between these factors and resolution has been confirmed. In addition to the extensive rearrangement of the crystal-packing mode, a number of bound glycerol and sulfate molecules are observed in the crystal structures of these mutants. These ligands unexpectedly provide additional packing interactions, for instance by producing a ligand-mediated hydrogen-bonding network at the crystal-packing interface. Notably, glycerol was not used as the crystallization reagent but was used as a cryoprotectant in data collection, suggesting that soaking crystals with suitable ligand solutions can improve crystal quality. Why are the outstandingly large overall structural changes relevant to the dramatic improvement in crystal quality? It is probable that the crystal-packing free energy of a mutant structure is only widely variable when its packing mode is very different from that of the wild-type structure. Thus, only a large structural difference which is, for instance, defined by the observed threshold levels (0.2 Å r.m.s.d. and 2.0° rotation) can provide markedly lowered crystal-packing free energy resulting in dramatically improved resolution. The second category of mutants providing unexpected results contained mutant crystals without outstandingly large overall structural changes and with increased packing interactions. Two mutations, N69K and E140R, provided crystals with slightly improved resolutions of 1.8 and 2.0 Å, respectively. In the E140R mutant structure, new intermolecular packing hydrogen bonds are formed with unexpected residues on the neighbouring dimer owing to a moderately large overall structural change. In the N69K mutant structure, the increase in conformational entropy arising from from the small-to-large mutation is compensated by the unexpected intramolecular anchoring as well as the unexpected creation of sulfate-mediated intermolecular hydrogen bonds that contribute to the crystal packing. The third category of mutants providing unexpected results contained the mutant crystals without outstandingly large overall structural changes and without increments in packing interactions. Three mutations, L65Q, E171R and K187R, provided crystals with slightly poorer resolutions of 2.2, 2.2 and 2.3 Å, respectively, indicating that the rational design of crystal contacts in the *Ph*DS system failed in these three of the 21 cases (14%) and that failure is not very destructive in terms of resolution. The 21 mutants in the *Ph*DS system can also be classified by the buried ASA at crystal-packing interfaces. A statistical correlation between the higher resolution (1.8 Å or better) group and higher values of buried ASA (4300 $Å^2$ or more) has been confirmed. The buried ASA value is a relatively good indicator of the strength of crystal-packing interactions. However, probably because the overall increase in packing area is not sensitive to the quality of interactions such as the geometry of hydrogen bonds and the cooperativity of van der Waals interactions, there are some exceptions, such as the mutants E54K, E140N, N142E and R173N. In future, the crystal-packing interactions should be

directly evaluated in free energy. To establish this, more detailed analyses using the *Ph*DS system or other model protein systems would be required.

In conclusion, the present study on crystal-contact engineering of *Ph*DS successfully proved that a systematic modification of crystal contacts by site-directed mutagenesis can improve the diffraction quality of protein crystals. The establishment of the *Ph*DS system allowed us to evaluate the mutation-induced change in crystal-packing interactions at the atomic level. When the crystal structure is available, the systematic approach as presented here would be useful for crystal-quality improvement. However, this study also showed that outstandingly effective mutations are difficult to predict rationally, indicating that some experimental screening method to select useful mutants may be desirable. Unfortunately, the present method is not helpful if the crystal structure is unknown. For such cases, an experimental technique to identify the crystal-packing residues should be developed.

HM crystallized all mutant proteins, determined/refined their crystal structures and wrote the paper, KS, SMMS, MNP, TK, BSKS, DKS and MRNM contributed to the refinement of mutant crystal structures and NK designed the experiments, evaluated the results and wrote the paper. We thank the staff of the RIKEN Structurome Research Group for assistance in protein production and M. Yamamoto and his staff for providing assistance during data collection on beamline BL26B1 of SPring-8. This work (PH0725) was supported by 'National Project on Protein Structural and Functional Analyses' funded by the Ministry of Education, Culture, Sports, Science and Technology of Japan.

References

Banatao, D. R., Cascio, D., Crowley, C. S., Fleissner, M. R., Tienson, H. L. & Yeates, T. O. (2006). *Proc. Natl Acad. Sci. USA*, **103**, 16230–16235.

Brünger, A. T., Adams, P. D., Clore, G. M., DeLano, W. L., Gros, P., Grosse-Kunstleve, R. W., Jiang, J.-S., Kuszewski, J., Nilges, M., Pannu, N. S., Read, R. J., Rice, L. M., Simonson, T. & Warren, G. L. (1998). *Acta Cryst.* D**54**, 905–921.

Chayen, N. E., Shaw Stewart, P. D., Maeder, D. L. & Blow, D. M. (1990). *J. Appl. Cryst.* **23**, 297–302.

Collaborative Computational Project, Number 4 (1994). *Acta Cryst.* D**50**, 760–763.

Cooper, D. R., Boczek, T., Grelewska, K., Pinkowska, M., Sikorska, M., Zawadzki, M. & Derewenda, Z. (2007). *Acta Cryst.* D**63**, 636–645.

D'Arcy, A., Stihle, M., Kostrewa, D. & Dale, G. (1999). *Acta Cryst.* D**55**, 1623–1625.

DeLano, W. L. (2002). *The PyMOL Molecular Graphics System.* DeLano Scientific, San Carlos, USA.

Emsley, P. & Cowtan, K. (2004). *Acta Cryst.* D**60**, 2126–2132.

Fisher, R. A. (1922). *J. R. Stat. Soc.* **85**, 87–94.

Kabsch, W. (1976). *Acta Cryst.* A**32**, 922–923.

Kishishita, S., Shimizu, K., Murayama, K., Terada, T., Shirouzu, M., Yokoyama, S. & Kunishima, N. (2008). *Acta Cryst.* D**64**, 397–406.

Kraulis, P. J. (1991). *J. Appl. Cryst.* **24**, 946–950.

Laskowski, R. A., MacArthur, M. W., Moss, D. S. & Thornton, J. M. (1993). *J. Appl. Cryst.* **26**, 283–291.

Lawson, D. M., Artymiuk, P. J., Yewdall, S. J., Smith, J. M. A., Livingstone, J. C., Treffy, A., Luzzago, A., Levi, S., Arosio, P., Cesareni, G., Thomas, C. D., Shaw, W. V. & Harrison, P. M. (1991). *Nature (London)*, **349**, 541–544.

Lee, B. & Richards, F. M. (1971). *J. Mol. Biol.* **55**, 379–400.

Luzzati, V. (1952). *Acta Cryst.* **5**, 802–810.

McElroy, H. E., Sission, G. W., Schoettlin, W. E., Aust, R. M. & Villafranca, J. E. (1992). *J. Cryst. Growth*, **122**, 265–272.

Merritt, E. A. & Murphy, M. E. P. (1994). *Acta Cryst.* D**50**, 869–873.

Otwinowski, Z. & Minor, W. (1997). *Methods Enzymol.* **276**, 307–326.

Ueno, G., Kanda, H., Hirose, R., Ida, K., Kumasaka, T. & Yamamoto, M. (2006). *J. Struct. Funct. Genomics*, **7**, 15–22.

Vagin, A. & Teplyakov, A. (1997). *J. Appl. Cryst.* **30**, 1022–1025.

Yamada, H. *et al.* (2007). *Protein Sci.* **16**, 1389–1397.

Yokoyama, S., Hirota, H., Kigawa, T., Yabuki, T., Shirouzu, M., Terada, T., Ito, Y., Matsuo, Y., Kuroda, Y., Nishimura, Y., Kyogoku, Y., Miki, K., Masui, R. & Kuramitsu, S. (2002). *Nature Struct. Biol.* **7**, 943–945.